The self-inversion of the sign of circular polarization in "halo" microwave sources

T.I. Kaltman, A.N. Korzhavin and N.G. Peterova
SAO RAS, St. Petersburg

Abstract.
The example of a large active region AR NOAA 5200 from October, 1988 is used to investigate the concept of the "halo", a magnetosphere-like structure above the active region. This structure is studied using radio spectral polarization observations with the high spatial resolution mainly obtained from radio telescope RATAN-600. In the case of AR 5200 the halo emission accounted for $> 50\%$ of the total AR emission. The results of the analysis of the observational data and of the model calculations allow to make the following conclusions: 1. The halo is a large non-structured source of emission with a size of the total AR, with the emission centered at the dividing (neutral) line of polarities of the bipolar sunspot group. 2. The emission spectrum allows to distinguish two components: a thermal part and a non thermal part. The presence of two types of the source implies that there are two populations of particles with different energy levels in the emission region. The phenomenon of inversion of the polarized halo radio emission could be explained by the influence of propagation conditions inside the source. The term of self-inversion is introduced. The maximum in the halo flux spectrum at the wavelengths 5 – 10 cm may be explained by Scattering due to the strong suppression of the emissivity of non-thermal electrons at these and longer wavelengths.

Keywords: Sun, circular polarization, microwave sources

1. Introduction

The phenomenon of the inversion of the sign of circular polarization was discovered by Piddington and Minnett (1951) practically simultaneously with the S-component of solar radio emission. The use of more recent observations mainly with moderate spatial resolution (Tanaka and Kakinuma, 1960; Peterova and Akhmedov, 1973; Maksimov and Bakunina, 1991) made it clear that this phenomenon had been observed in the majority of local sources($> 50\%$) of S-component. Taking into account frequent changes of the sign of the polarization in the burst emission (Tanaka and Kakinuma, 1959; Kruger, 1976) we can consider this phenomenon to be one of the characteristic features of solar radio emission.

It is known that ordinary and extraordinary wave modes emitted by thermal plasma or by an ensemble of mildly relativistic electrons generally have elliptical polarization (Zheleznyakov, 1964; Kundu, 1964). In the source region the sign of circular polarization corresponds to the sign of the longitudinal component of the magnetic field. This makes it possible to determine the magnetic field polarity in the source on the basis of its circular polarization if the sign of circular polarization should be preserved until the emission reaches the observer.

Wave propagation effects and the inversion of the sign of the polarization in QT-regions have been studied by many authors (Cohen, 1960; Zheleznyakov and Zlotnik, 1963; Bandiera, 1982; Alissandrakis and Preka-Papadema, 1984; Peterova, 1997). The result depends on the degree of coupling between the two wave modes. In the case of weak coupling each mode propagates independently of the other and its polarization at each point of the propagation path depends on the local conditions.

For weak-coupling propagation through a QT-region (i.e. the region with quasi-transversal magnetic field) the sign of circular polarization inverts due to the inversion of the longitudinal component of the magnetic field. However, within the limits of strong coupling the sign of the circular polarization does not change during propagation through QT-region. The coupling is strong for frequencies much higher than the critical frequency (Zheleznyakov and Zlotnik, 1963):

$$f_c \approx \left(2 \cdot 10^{17} N_e B_0^3 \frac{1}{\left|\frac{d\theta}{dz}\right|}\right)^{1/4} \qquad (1)$$

where N_e – the density of thermal electrons, B_0 – the strength of magnetic field, $\frac{d\theta}{dz}$ – the scale of magnetic field divergence. The QT-inversion phenomenon is purely geometrical: the sign of circular polarization depends on the heliographic coordinates of the emission source and inverts after passing the central solar meridian. Therefore this phenomenon has been interpreted as the influence on the polarized emission of propagation conditions in the magneto-active medium of the solar corona (Piddington and Minnett, 1951). The theory of this effect was developed by Cohen (1960) and Zheleznyakov and Zlotnik (1963). Until now, it has commonly been used to refer to the influence of transversal magnetic fields for events with dominant ordinary mode. However, the analysis of the observations with high spatial resolution (Peterova, 1997) has shown that this theory could be applied only to *the sunspot component* of the local source structure.

The observations with the high spatial resolution made with RATAN-600 showed that the strong magnetic fields of the sunspots are not the unique source of the S-component. Apart from the compact sunspot component there is a large emission source with the size of about that of the whole AR. This source is identified as a large volume of plasma confined by the magnetosphere of the active region. This type of source has been singled out by Korzhavin in (Kaltman et al., 1998) as a separate class and has been called "halo" source. It was revealed that the halo makes an essential contribution to the total emission of the local source: about 50% for a typical case (Peterova, 1994). The polarization of the halo (Korzhavin and Peterova, 1992) has some characteristics not well explained by the classical QT-theory developed by Cohen (1960) and by Zheleznyakov and Zlotnik (1963).

In the next section the experimental and theoretical investigation of the halo is presented with the example of the AR 5200 (October, 1988) because the emission of this region consists mostly ($\approx 80\%$) of halo emission.

Recently this region was discussed by (Sych et al., 1993), where the structure of AR 5200 was interpreted as an example of a "cold" peculiar source. This does not conflict with our new interpretation since the halo, along with peculiar sources, belongs to one class of sources above the neutral line.

Here for the first time the modelling of the polarized emission takes into account the inverse effect due to the influence of transverse propagation of the emission inside the source itself. This effect we have called "the self-inversion effect". The introduction of this term allows us to put in order our conception of the inversion of the sign of the polarization and to divide it into two categories: for the compact sources of cyclotron emission (the sunspot sources, each unipolar) and for the large halo-like bipolar sources. As we can see from the observations, the separator between these categories and their sphere of action lays in the wavelength range $\lambda_{bound} \approx 5$ cm: the first type (of "classical" QT for sunspot emission) is predominant for the wavelengths shorter then λ_{bound}. For the longer wavelengths the character of the polarization is determined by the self-inversion inside halo-like bipolar sources.

2. Observations of AR 5200

The solar observations made with the radio telescopes RATAN600, Large Pulkovo Radio telescope (LPR) and SSRT (Siberian Solar Radio Telescope) in both one dimensional and two dimensional regimes were used in these studies. For our task an investigation of the solar sources like halo it is very important that these instruments provide the detection of extended parts of the radio sources with the size of about the whole active region of 2 – 4 arc min located in the corona above active regions.

A brighter ($T_b \approx 2 - 4$ MK) and more compact (about 20 – 30 arc sec) sunspot associated component may be detected against the background of the halo with the accuracy which depends on the spatial resolution of the instruments. For the RATAN-600 radio telescope the E – W resolution is 17 arc sec at the wavelength of 2 cm and for SSRT it is 20×20 arc sec (the size of the synthesized diagram at 5.2 cm).

The choice of the active region AR 5200 (latitude $\psi = 21^o$, central meridian passage CMP on October 24, 1988) was determined by the following parameters:

1. The AR 5200 had a large area (up to S_p = 1800 x10^{-6} of solar hemisphere) and extent was about 4 arc min in moment of CMP, i.e. the spatial resolution of the used instruments was enough for investigation of its structure.

2. Its large scale magnetic structure was bipolar which allowed us to study the interspots space.

3. The evolution of the group was rather smooth: the leader spot was gradually splitting and in CMP it was like a symmetrical group the leading and tailing parts of which consist of many little spots.

4. There were no deltaconfigurations, which resulted in the absence of bright peculiar details, which could interfere with the investigations of the halo. This fact is in agreement with a very surprisingly weak flaring activity in such a large active region.

To identify the details of the local source we used the original photoheliograms obtained at the Kislovodsk observatory (GAS). The processing of the observational data was made by the methods usually applied at RATAN-600 and LPR radio telescopes (cite Bor87 – cite AkhmedCAO).

AR 5200 was observed from the rising to the setting. Its offlimb emission was observed during $\pm$ 2 days which shows that its emission region spread high into corona (up to 10^5 km).

The results of observations can be seen in Figure 1 and Figure 2. The RATAN-600 scans are shown for the moment of CMP of AR 5200, which is the best for studying the structure of local source. To study the dynamics of the local source it is better to use the SSRT which has a better spatial resolution at 5 cm than RATAN-600.

The structure of the polarized emission source and especially that of non polarized emission(Stokes parameter V and I) were found to be unusual. The maximum of the brightness distribution was near the neutral line of the AR and coincided with the no one of maximum of polarized emission. The sunspot associated component was detectable only at the wavelength of 4 cm. It looked as weak details in intensity

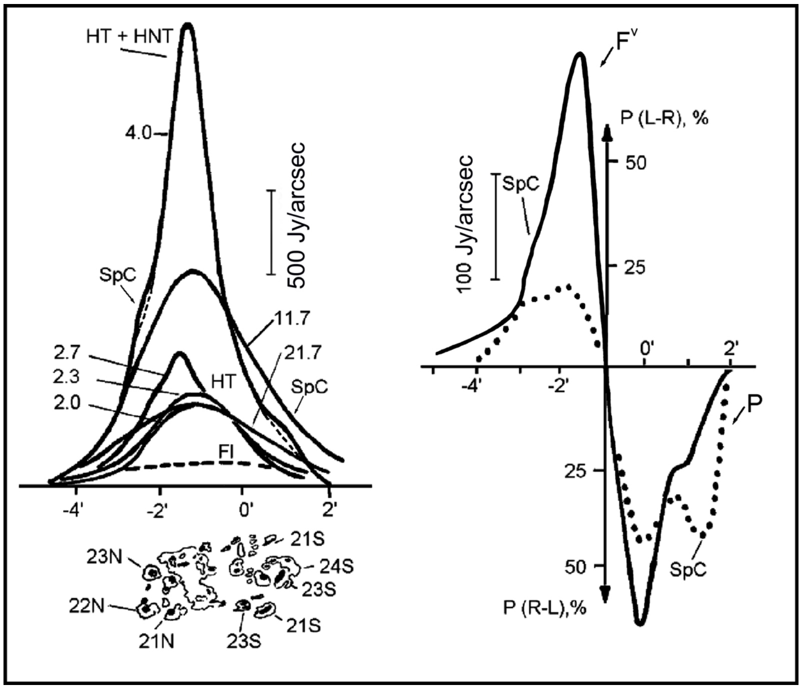

Figure 1. The one-dimension scans of AR 5200 in the intensity I (to the left) and the circular polarization V (to the right) channels as measured with RATAN-600 observations on October 24, 1988 superposed with the photo heliograms of Kislovodsk station.

(on the scans denoted by SpC), which accounted for the less than 20% of the whole emission of the local source. They coincided with the largest spots in the sunspot group favorable situated at its (E – W)-edges. That can be seen at the scans in the channel V, especially on the curve denoted by P - degree of polarization. The halo-type source was responsible for the main part (about 80%) of the emission. In the local source structure of AR 5200 the following details can be detected:

1. A wide source with an effective size $\approx$ 5 arc. min., probably of floccular origin, (the detail Fl in Figure 1). This detail can be clearly seen in range 2.0 – 2.7 cm and has a flat spectrum F^i ($\approx$ 5 sfu), a relatively low polarization degree P (8 – 10%) for the both components of the bipolar structure of the polarized image.

2. A "thermal halo" is also a rather elongated source (detail HT in Figure 1) with the sizes 2.0 – 2.5 arc min and it is associated with the space between sunspots. The spectra F^i and the polarization of the emission are similar to the floccular source. The thermal halo was a rather stable component during the whole period of

observing, its flux beeing about 5 s.f.u. at shortest wavelengths. At the rising of AR (17/X –1988) The height of the source in corona was estimated as ≈15 thousand km (for the wavelength of 2,3 cm).

3. A "nonthermal halo" (the detail HNT in Figure 1) was clearly distinguished only at the wavelengths more than 2.7 cm. Its position (for example, on 24/X) approximately coincided with the neutral line of the magnetic field. Its sizes is increasing with increasing of wavelength from ≈ 0.7 arc min at 2.7 cm to 2.5 arc min in range (10.7 – 21.7) cm.

   The emission spectrum of this detail was characterized by a very steep (up to 10 times) increase from short to long wavelengths at about (3 – 4) cm which explains the term non thermal halo. Figure 1 shows that the non thermal halo has maximum in brightness distribution along the local source at 4.0 cm. The flux of this detail was of about ≈ 18.5 sfu at the wavelength 4.0 cm and 3 times as much as that of the core components (≈ 7.0 sfu, SpC). At that time period the non thermal halo emission was to more then 50% of total local source emission (≈ 35 sfu). For the time when the AR appeared at the limb the height of the effective center of the emission at the wavelength 4.0 cm was estimated to be ≈ to 30 thousand km above the photosphere, and the total emission region reached the high up to 100 thousand km.

   At central meridian passage the polarization image of the non thermal halo had a bipolar structure. Non of its peak coincided with those of unpolarized emission. The one-dimensional degree of polarization in Figure 1 was rather high (P=20% and 45%) as it is typical for a sunspot component. However, the described emission regions with the maximum degree of the polarization did not coincide with the sunspots and were shifted towards the center of the AR.

The brightness distribution of the polarized emission shows bipolar structure only for $\approx \pm 2.5^d$ near to the central meridian. During the moving toward the limb the source becomes unipolar, but the sign of the polarization of its emission is different on the $E-$ and on $W-$ limbs. The main features of this process can be seen in scans sequence (Figure 2 made with the SSRT (Solnechnye Dannye, 1988, 10). As shown in Figure 2, close to the $E-$ limb a wide source is observed in the polarized emission. A brighter detail associated with the leading sunspot which has not yet decayed (as mentioned above) stand out sharply against a background of the wide source. This detail is shown by hatching in Figure 2. The brightness maximum of the wide detail in

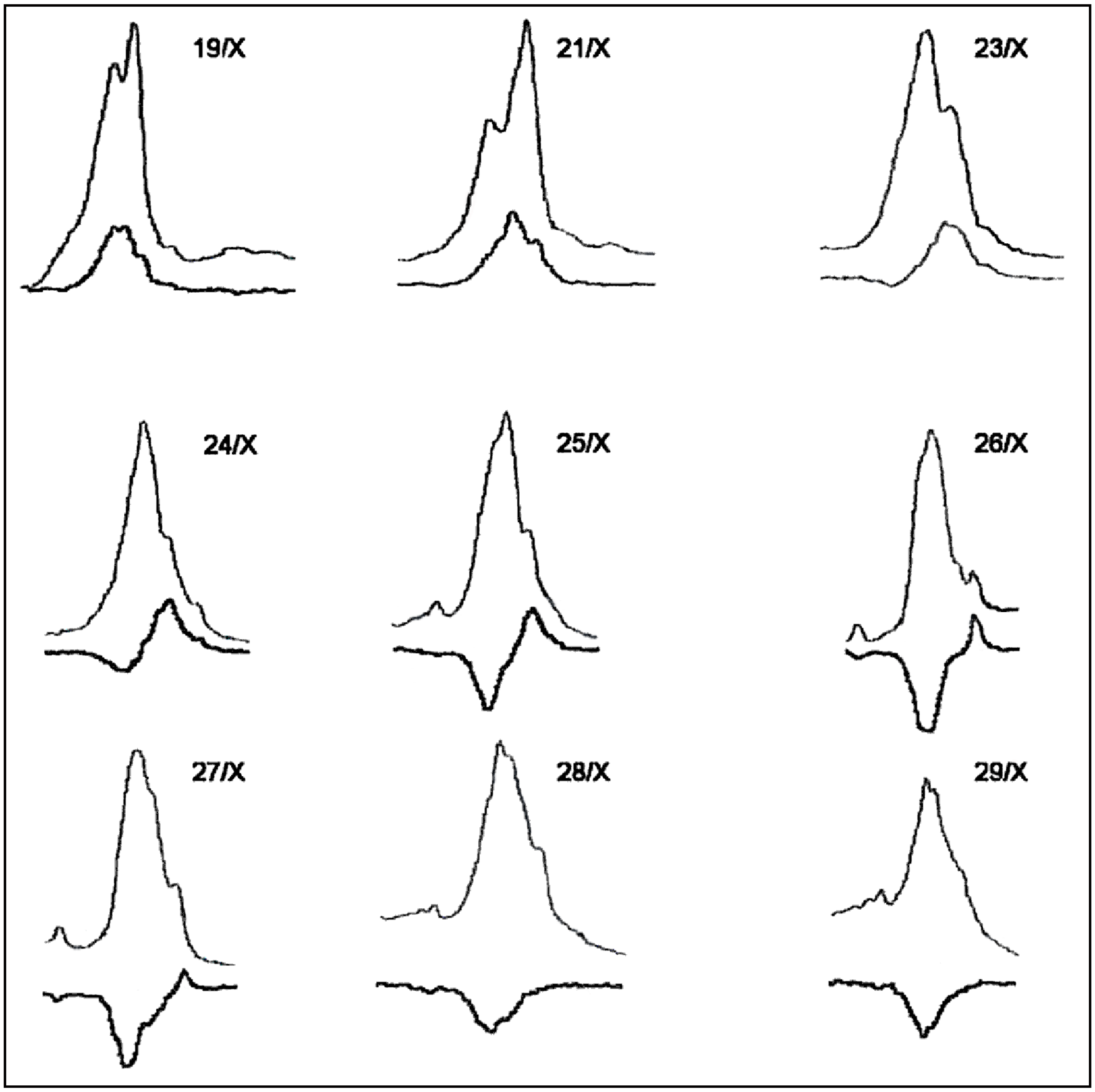

Figure 2. The one-dimension scans of R 5200 in the intensity I and the circular polarization V channels as registered with the SSRT observations at the wavelength 5.2 cm on 19/X - 29/X 1988

V-channel approximately coincides with that in intensity, and the sign of polarization corresponds to an extra-ordinary mode of emission for the magnetic field in the leading part of the AR. While approaching to the central meridian the brightness distribution of the local source polarized emission becomes bipolar. Sign of both components corresponds to the sign of the magnetic field of the leader and tail parts of the AR. However, as mentioned above, no maximum coincides with the maximum of the non polarized emission. As the AR approaches to the $W-$ limb, changing of the polarized image structure of the wide detail executes in the reverse order – the source becomes unipolar again, but its polarization sign corresponds to the excess of the extra-ordinary emission for the magnetic field of the tail part of the AR. Near to the $E-$ and $W-$ limbs the shape of the brightness distribution along the wide source of polarised emission is close to a gaussian but it is asymmetric, with a rapid decrease on the side closest to the disk center.

As the above description shows the behaviour of the halo polarized emission is of a geometrical character. It means that in this case the influence of the propagation conditions on the polarized emission in the bipolar magnetic field of the AR takes place also. However, as opposed to the compact sunspot associated component, we deal here with a spatially extended emission source, for which the region of the transversal magnetic field and waves transformation is not outside, but inside the source itself. The main change of the polarization sign lasts about 5 days, while for the compact sunspot associated component (seen below Figure 5) this process takes less than one day.

To study the polarization inversion phenomenon for halo type sources we used the AR, in structure of which halo is dominant. In reality the structure of the most ARs is much more complicated. In each case the brightness distribution is determined by the ratio of the contribution, which every component makes into the total emission. By way of example, here we present the observations of the AR NOAA 9280 (see Figure 3, 4) made with the SSRT in twodimensional regime. The SSRTmaps are related to the SOHO magnetogramms and photoheliogramms. The correlation shows that the observed brightness distribution is due to the contribution both sunspot associated details and halotype source. That is way maxima in intensity and polarization are shifted out of the sunspot position. At the same time a wide component of local source structure is evidently separated from total structure. Dynamics of its polarized image shows the same regular trends which were perceived in the onedimensional observations of the AR 5200.

To stress the peculiarities of local source structure of AR 5200 we provide an example of the structure, in which the sunspot associated details are dominant. To illustrate this, an active region (AR 8230) with a simple morphology was chosen (see Figure 5). The SSRT-observations at a period of polarization sign inversion in the tail detail are presented. As Figure 5 shows inversion lasts less than a day. On April, 5 depolarization line (zero point) is projected into the tail sunspot and divides polarized source in two parts. The depolarization line at the wavelength

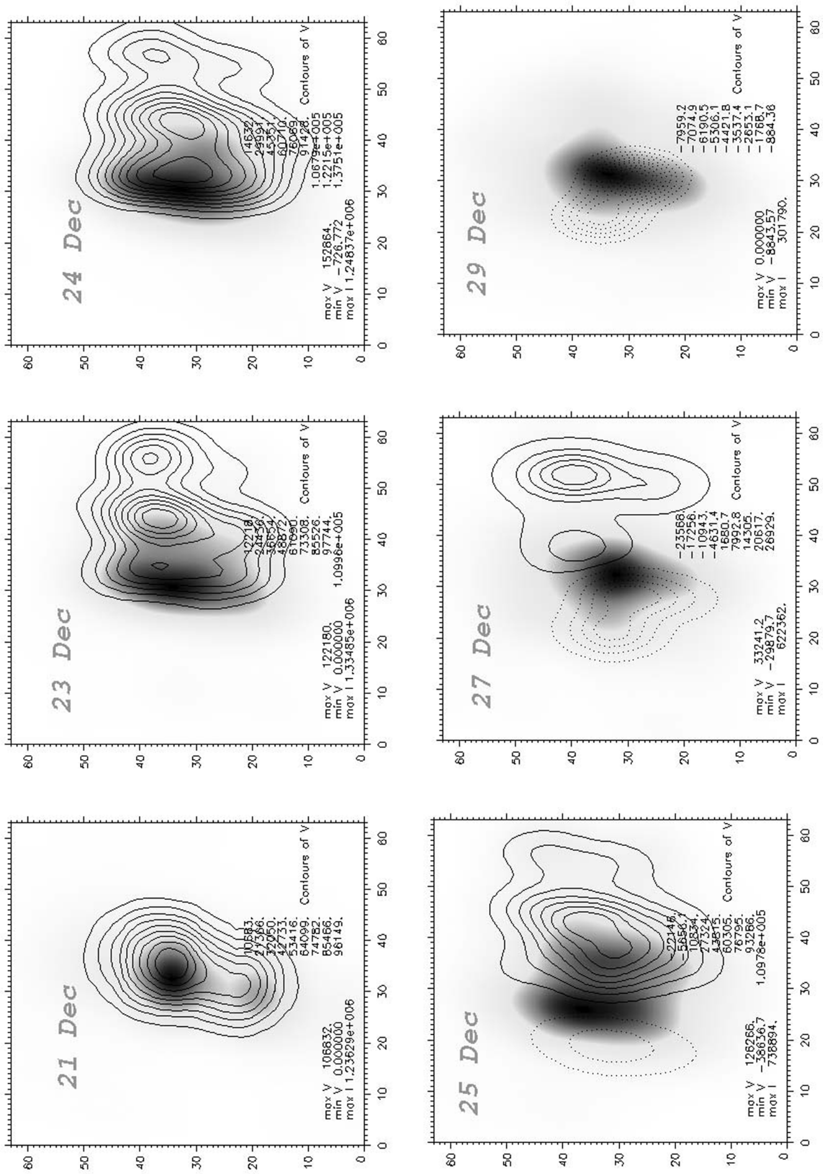

Figure 3. The SSRT-maps of the AR 9280. Intensity is shown as grey scale image, polarization (R-L) - solid lines, (L-R) - dotted lines.

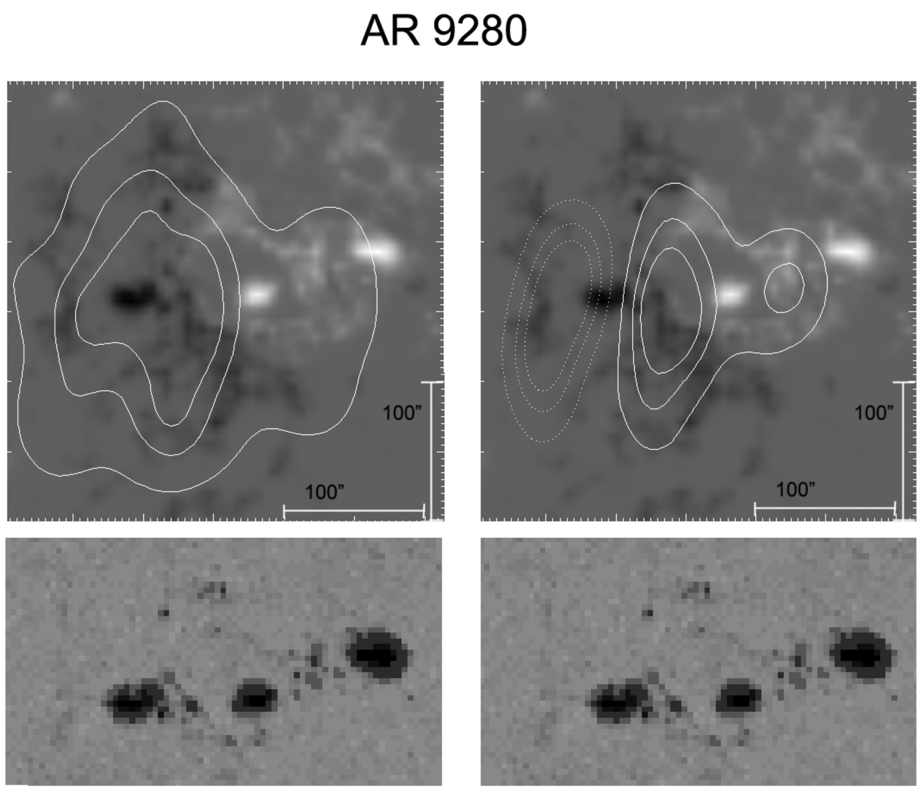

Figure 4. The SSRTmaps are related to the SOHO magnetogramms and photoheliogramms. Top: magnetogramm is shown as grey scale image overplotted by intensity SSRTmaps (to the left, contours) and by polarization SSRTmaps (to the right, (R-L) - solid lines, (L-R) - dotted lines.

5.2 cm (SSRT) corresponds to the coronal magnetic field of about 20 Gs.

What are the physical parameters of the plasma generating the halo emission with the described features? We can try to answer this question modelling the loop structure of the solar corona. This problem will be solved if the model will explain the main characteristics of the halo emission provided by the observations. Here it should be noticed that the greatest difficulties in calculation were connected with the modeling of the halo emission in intensity.

The main characteristics of halo type source as infered from observations of AR 5200:

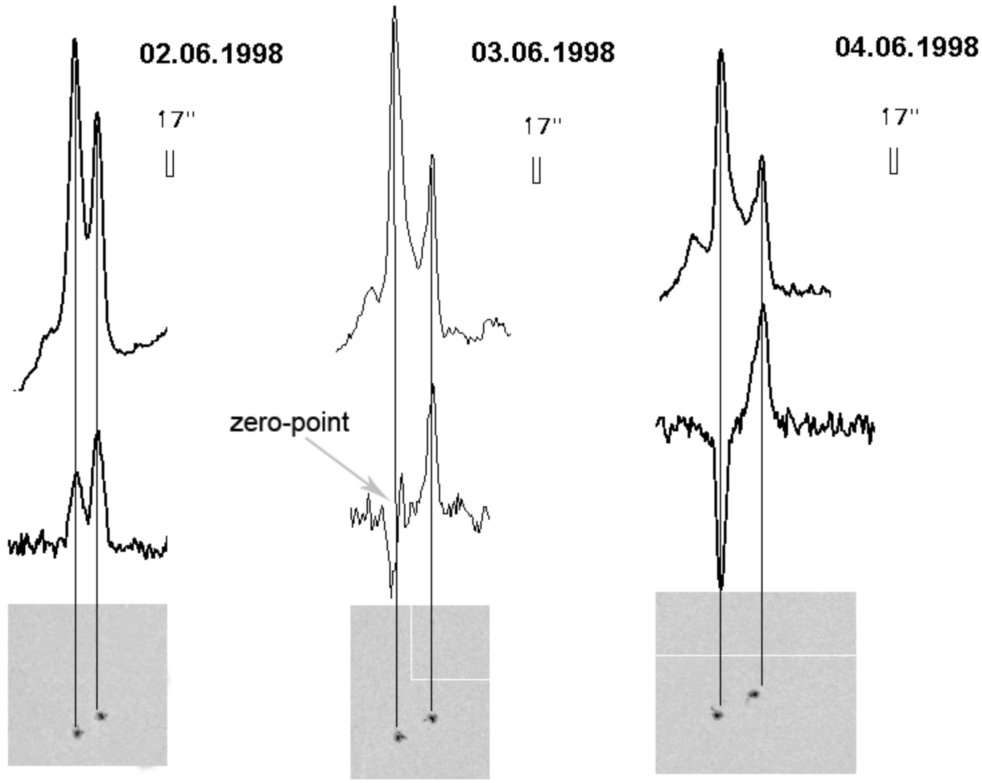

Figure 5. The SSRT-scans of the AR 8230 are related to the SOHO photoheliogramms

- The halo contribution (a broad non structured source with sizes 3'–5') to the total radio emission of the great active regions is more then 50% in the range 2 – 30 cm. In the case of the AR 5200 the compact sunspots associated sources, usually well observed at the shortest wavelengths (2 – 5 cm), are attenuated or absent.

- In halo spectrum (see Figure 7) we distinguish next parts: a) a flat thermal part at the shortest wavelengths (2 – 3 cm) with flux level $\approx 2-5$ sfu; b) a steep rising part (spectral index $n \simeq 6$) at the wavelengths range 3 – 5 cm; c) a maximum part, where the flux equals $\approx 20-50$ sfu at the wavelengths 5 – 8 cm; d) a descending part at the longer wavelengths with the spectral index $n \simeq -1$. The halo brightness temperature reaches to 3 – 5 MK.

- The halo emission has a very week directivity. The limb observations give the effective height of the halo type source about 30 – 50 thousand km above the photosphere.
- The brightness distribution of the halo polarized emission close to the central meridian (2 – 3 days after and before the central meridian passage) has the symmetrical bipolar structure corresponding in terms of polarization sign to the predominance of extra-ordinary wave accordingly to the photosphere measurements of the magnetic field. At the rising and at the setting the halo polarized emission is observed as a unipolar source of an asymmetric shape with the sign of the polarization corresponding to the predominance of extra-ordinary mode for the magnetic field – of the leader part of the AR close to the E-limb and of the tail part of the AR close to the W-limb. The polarization degree of the halo in range 3 – 5 cm (the steep increasing of the flux) is rather high (up to 50%), which is usually believed typical only for the sunspots associated component of the AR microwave structure.

3. Model calculations

To model the observations, we used 3-D calculations of thermal and gyro synchrotron emission from electrons encased in a big coronal loop with strong magnetic fields representing the magnetosphere of the AR. The following parameters were chosen for electron populations filling the magnetic loop: the kinetic temperature T_e and the density N_e of thermal electrons, the density N_0 of non thermal electrons at the lowest limit of energy $E_0 = 10$ keV and the spectral index δ.

The equation of energy transport was solved inside the source region (see Appendix, A). The complete equations (Zheleznyakov, 1964) for free-free mechanism (see Appendix, B) and the approximation equations (Dulk and Marsh, 1982), with modifications (Dulk, 1985), for gyrosynchrotron emission from thermal electrons (see Appendix, C) and from nonthermal electrons (see Appendix, D)were used for the calculations.

The integration was carried out with a variable step permitting calculation of an increment of optical depth not exceeding 0.01 at every step. It was assumed that there were neither absorption nor emission above the source. The quiet Sun contribution was supplied as the initial value of the intensity at the base of every line of sight.

The dipole approximation was used for to calculate the magnetic field. The loop was modelled by force lines of magnetic field of two

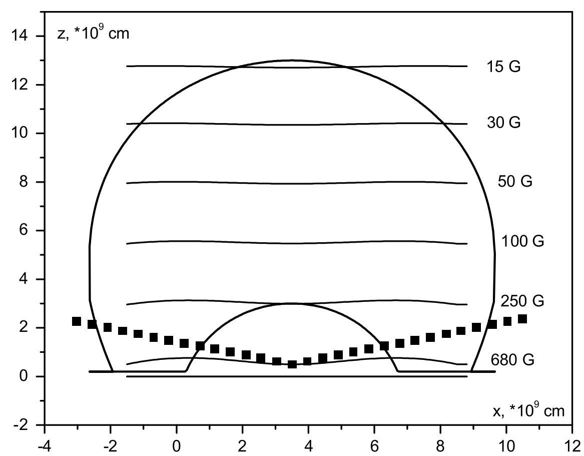

Figure 6. The structure of halo magnetosphere presented as a 3D magnetic loop, z-the height above photosphere.

dipoles spaced by 7×10^9 cm. The calculated source sizes equaled to 1.8– 2.3 arc min, corresponding to the observed halo sizes equaled to 2.0 – 2.7 arc min. The maximum value of the magnetic field at the dipole axis was taken to be 1000 G. The source model with the magnetic force lines is presented in Figure 6. The sunspot component makes the main contribution to the strong magnetic fields close to the dipole axis (at the feet of the loop). To limit the contribution of the sunspot emission to the model, we cut off in calculations the loop parts confined by a cone whose top was placed at the photosphere on the dipole axis and with a cone opening 15^o. The cut-off part is below the line marked with squares.

For thermal electrons the following parameters were taken: the temperature of thermal electrons is $T_e = 3.7 \times 10^6 K$, the density of thermal electrons is $N_e = 2.0 \times 10^9/\mathrm{cm}^3$.

For non thermal electrons the choice of parameters was more complicated since no choice gave a satisfactory agreement with the observational results. The calculations were made for several models. The results of the spectrum calculation are presented below for two of the most satisfactory models.

The calculated spectrum is compared to the observed one in Figure 7, where the results of the calculations for the two models are presented. For model 1 the density of non thermal electrons is $N_0 = 1.7 \times 10^7/\mathrm{cm}^3$ and the spectral index is $\delta = 5.3$. This model agrees well with the observations at wavelengths shorter then 4.0 cm. But the ratio of the

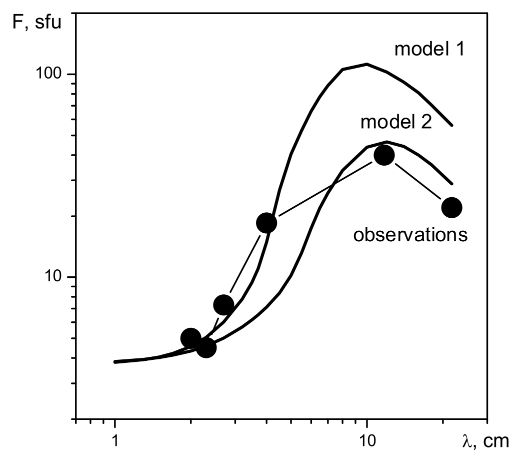

Figure 7. Flux spectrum of halo emission observed on October 24, 1988 and calculated (models 1 and 2).

total density of non thermal electrons energy to the density of thermal electrons energy $W^{nt}/W^{t} = 0.35$, which is extremely high.

For model 2 the density of non- thermal electrons is $N_0 = 1.7 \times 10^5/\mathrm{cm}^3$ and the spectral index is $\delta = 4.3$. This model agrees with the observations at the wavelengths 2.3 and 11.7 cm, but it has too small flux values in the intermediate wavelength range. The ratio $W^{nt}/W^{t} = 0.004$ in model 2 is more realistic. Possible explanations of the discrepancy between the observed and model spectra will be discussed below.

3.1. The influence of propagation effects on the sign of circular polarization

To model the polarized emission of the halo, the effects of propagation through the QT-region of magnetic field inside the emission source were taken into account. It should be noted that such conditions are common for large coronal loops.

The possible inversion of the sign of polarization for propagation of the emission through QT-region was taken into account by Allissandrakis and Preka-Papadema (1984) for a flaring loop. Their model loop had the same configuration as our one, but they calculated only the QT-regions situated outside the source.

According to our modelling, one-dimensional calculated distributions of the emission intensity along the source are presented in Figure

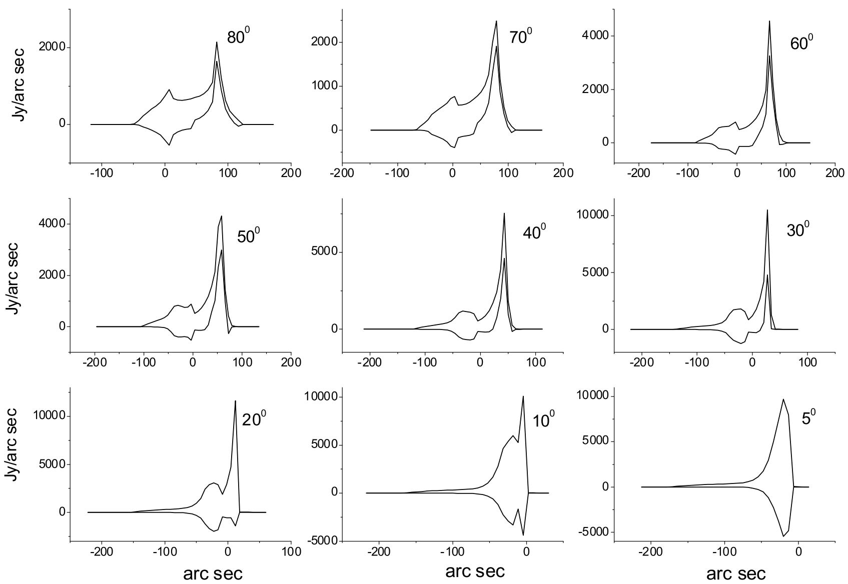

Figure 8. The one-dimensional calculated distribution of the emission intensity along the source at 5 cm for the total and polarized emission without a diagram pattern convolution.

?? for the total and polarized emissions at 5 cm. Profiles were calculated for different positions of the source on the western part of the solar disk (the most western position was at a longitude of 85^o). The calculations presented in Figure **??** were made without convolution.

The calculated one-dimensional distributions of the intensity along the source at 5 cm for the total and polarized emission after SSRT beam convolution are presented in Figure 9. The calculations of polarized emission without taking into account the inversion effect are marked by the dashed line. One can see that the self-inversion effect strongly affects the character of the distributions of polarized emission along the source. The inversion of the polarization sign starts in the leading part of emission distribution at western longitude of 20^o, and then the source becomes unipolar at western longitude of 70^o. The same inversion effect takes place in eastern hemisphere, but the tailing part is now inverted. A comparison with the results of the observations shows that the model is good enough to present the main peculiarities of the polarized emission distributions depending on the AR longitude. The major discrepancy concerns the non polarized emission, which has the observed maximum above the neutral line while the model shows a

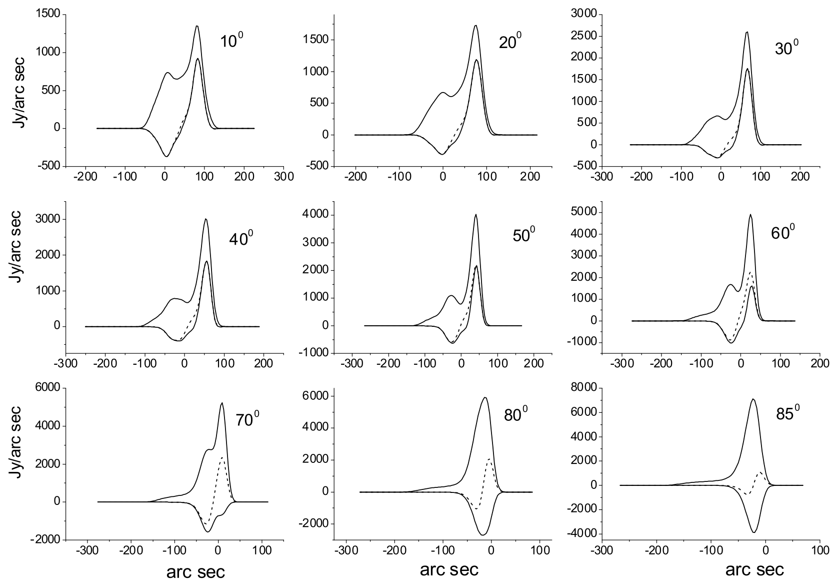

Figure 9. The one-dimensional calculated distribution of the emission intensity along the source at 5 cm for the total and polarized emission after SSRT diagram pattern convolution. The calculations without taking inversion effect into consideration are marked by dashed line.

curve with two maxima: above the leading and trailing sunspots. The discrepancy is likely to be explained by taking into account the effects of scattering.

Indeed, if we take into consideration the scattering effect on radio emission propagating through the halo medium at longer wavelength ($\lambda > 5$ cm), the scattering coefficient is $\sigma \sim \lambda^4$, for some types of plasma turbulence. The nonthermal electrons lose their energy and this leads to exciting the plasma waves which results in the effective scattering of the radio waves propagating through the coronal loop, with a strong dependence upon the wavelength. For more details about the plasma waves scattering see in Appendix, E.

Such scattering can explain the following effects:

– the presence of the maximum in the spectrum of the halo flux in the wavelength range of (5 10) cm due to strong depression of the emissivity of nonthermal electrons at these and longer wavelengths. This is a region of the opacity of the halo matter due to scattering.

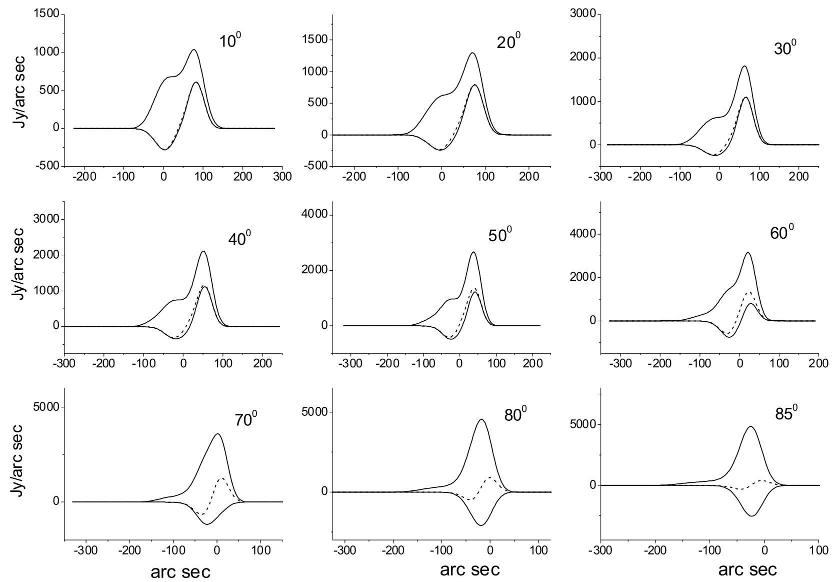

Figure 10. The one-dimensional calculated distribution of the emission intensity along the source at 5 cm for the total and polarized emission after double SSRT diagram pattern convolution. The calculations without taking inversion effect into consideration are marked by dashed line.

– the steep part of the halo spectrum in the range of mid opacity (3 – 5 cm). Here are, in fact, the total emission of the halo and the sunspot component, with the sunspot component being fuzzy due to scattering throughout the halo volume.

– at the shortest wavelengths (2 – 3) cm both the scattering and nonthermal contribution are negligible, therefore only the emission of the optically thin thermal coronal plasma is observed.

The calculated distributions of the intensity along the source in Figure 9 were made without taking scattering into consideration. It is known that scattering can lead to increasing angular dispersion of the source emission propagating through the turbulent plasma (Kaplan and Tsytovich, 1972; Tsytovich and Kaplan, 1984), or through the interplanetary medium (Bastian, 1994). After accounting of the scattering, the modelled double-humped distribution of brightness along the source became smoother and more corresponding to the observations.

The scattering effect is, in some way, similar to a degradation of spatial resolutions in the observations. In Figure 10 the one-dimensional calculated distributions of the emission intensity along the source are presented after double SSRT beam pattern convolution. One can see that after this double forced convolution with the larger beam the distributions become more similar to the observed ones (Figure 2), then after the convolution with the real beam (Figure 9). This convolution with the larger beam is equivalent to the possible influence of scattering leading to the angular dispersion of emission.

According to the observations, the magnetic field has to be stronger then in the model coronal loop. The calculated value of the polarization degree of gyro synchrotron emission is $5 - 20\%$, which is consistent with the observations at all wavelengths except the range $3 - 5$ cm , where the steep increase of halo flux is observed. The high degree of polarization observed here may be explained by the scattering addition of the sunspot component, as the true polarization degree of the sunspot component can reach 100%.

Another possibility to correct the discrepancy between 2-peak modeled distributions and 1-peak observed ones is to change the construction of the model source. Positions of the boundary arcs of the model loop (see Figure 6) are the free parameters of the model. The extension of the top boundary of the arc does not significantly affect the model distribution of radio emission along the source. On the contrary, the position of the bottom boundary arc is more important because of strong magnetic field. We placed the lower level of the loop into the chromosphere and did not change any other parameters of the model. The maximum of the magnetic field was placed between the loop legs. In this way we modeled the unique maximum of cyclotron emission source, see Figure 11. The unique maximum of the emission between the legs of the loop should be modeled in the similar way for the magnetic loops under the following conditions: the loop legs are strongly inclined to the photosphere and situated closely to each other.

4. Discussion

Existence of wide loops in the solar AR magnetosphere is under consideration. The radio astronomy observations made by RATAN-600 and VLA telescopes with high spatial resolution show only wide non structured sources at the long wavelength part of the research range, with small fraction (less then 5%) of possible fine structures (Akhmedov et al., 1987). On the contrary, TRACE, RHESSI, YOHKOH registered very thin X-ray and EUV loops.

The results of the one-dimensional RATAN-600 observations were confirmed by SSRT observations made in a cartography mode. SSRT

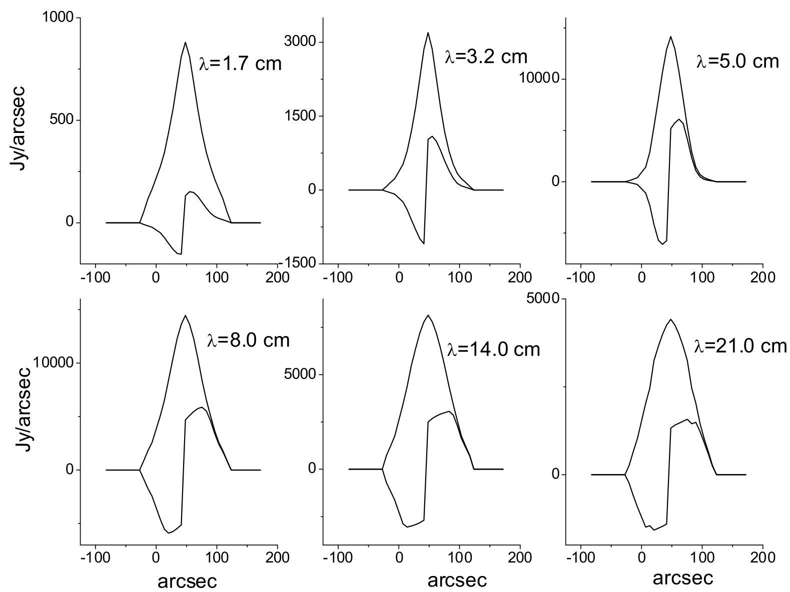

Figure 11. The one-dimensional calculated distribution of the emission intensity along the source in the center of solar disk at 1.7, 3.2, 5.0, 8.0, 14.0, and 21.0 cm for the total and polarized emission without diagram pattern convolution.

maps at 5 cm show a local source as a loop with the maximum of emission above a neutral line as a rule. At the feet of the loop bright sources of big sunspots can be seen. These sunspot sources could be interpreted as cyclotron sources emitting through the plasma which forms a halo-like source at the loop top. The contrast between these two types of sources depends on the halo opacity. In fact, we do not know the spectrum of the cyclotron emission source at the wavelengths longer than 5 cm, since it cannot be separated from the spectrum of the halo source.

The recent investigations of a coronal structure above a active region in the radio range, X-ray and EUV regions reveal that the real loop structure is much more complicated than the model used here. Evidently, it is necessary to take into consideration both an inhomogeneous distribution of temperature and density as well as a non dipole character of the magnetic field. We expect that this will result in a better agreement between the observations and the modelling, which leads to a significant refinement of physical parameters of coronal plasma. Simultaneously it opens up new possibilities for diagnostics of high temperature plasma and for forecasting of flare events.

5. Conclusions

Using the example of the large active region AR 5200 observed in October, 1988, the concept of the "halo" (i.e. a feature of the local source structure genetically connected with the AR magnetosphere) is studied using radio spectral polarization observations with the high spatial resolution (mainly of RATAN-600). In case of AR 5200 the halo emission accounted for $> 50\%$ of the total AR emission. The results of the analysis of both the observational data and the model calculations allow us to make the following conclusions:

1. The halo is a large non-structured source of emission with the size of order of the total AR, with the emission center at the neutral line. The position of the emission center can be slightly varied due to changes in the AR morphology, often shifting to the fragmenting part of the AR.

2. The spectrum of non-polarized emission allows us to distinguish two components: a thermal part and a non thermal part. The thermal free-free emission with a flat spectrum (or a descending one at the longer wavelengths) is observed at wavelengths shorter than 2.7 cm. Starting from the wavelength ≈ 2.7 cm the non thermal addition with a very steep spectrum in the range 3 - 5 cm and with a smoothed maximum at 7 - 10 cm becomes apparent. This proves that there are two populations of particles with different energy distributions in the emission region.

3. The halo emission is polarized and shows inversion of the sign of polarization depending on the heliographic longitude of the AR. The phenomenon of inversion in the halo could be explained by the influence of propagation conditions on the polarized emission inside the source of this emission. The term "self-inversion" is introduced.

4. The investigation of the halo polarization leads to a further development of the concept of the polarization sign inversion in the local source emission. Two features can be distinguished: the inversion for the cyclotron emission sources observed at a short part of the spectrum (< 5 cm), and the self-inversion for halo determining the character of polarization at the longest wavelengths (> 5 cm).

5. A model source presented as a big coronal loop containing thermal electrons and non-thermal electrons with a power-law energy distribution is used to model the effects of propagation through the QT-region of the coronal magnetic field. The model well explains the main characteristics of the phenomenon of the inversion in the halo. The observed characteristics of halo emission could be explained with the following model parameters: the temperature of thermal electrons $T_e \approx 4 \times 10^6 K$, the density of thermal electrons $N_e \approx 10^9/\text{cm}^3$, the density of non-

thermal electrons $N_0 \approx 10^5/\text{cm}^3$,the spectral index of non-thermal electrons $\delta = 3 - 4$, the magnetic filed strength $H = 400 - 50$ G.

6. Scattering can lead to a maximum in the halo flux spectrum at wavelengths 5 – 10 cm due to the strong suppression of the emissivity of non-thermal electrons at these and longer wavelengths (this is a region of high opacity of the halo matter due to scattering). The steep part of the halo spectrum in the range of half-opacity (3 – 5 cm) is being, in fact, the total emission of the halo and the sunspot component. The sunspot component is spatially fuzzy due to scattering throughout the halo volume.

7. Setting aside the problem of the sources and mechanisms of generating high energy particles as well as the problem of trapping and accumulation, one can note that in the case of AR 5200 the coronal loop was supported by a strongly fragmented structure at the photospheric level and, in fact, consisted of many single loops. Between these single loops favorable conditions could be realized for the formation of current sheets. The resistance instability of the current sheets, in turn, could generate the hot particles in quiescent regime filling this AR magnetosphere and making the halo so prominent. This assumption was confirmed by RATAN-600 observations which often revealed the diffuse brightening of the radio emission above bunches of small sunspots and pores.

Appendix

A. Equation of energy transfer

The transfer equation for the brightness temperature T_b and for the effective temperature T_{eff} along the path in isotropic medium for each mode of emission is (Zheleznyakov, 1964):

$$\frac{dT_b}{d\tau_\nu} = -T_b + T_{eff} \tag{2}$$

where the optical depth τ_ν can be found by integration of absorption coefficient κ_ν along the path l:

$$\tau_\nu = \int_0^l \kappa_\nu ds \tag{3}$$

After integration of the equation (2), we receive:

$$T_b = \int_0^{\tau_\nu} T_{eff} e^{-t_\nu} dt_\nu + T_{bo} e^{-\tau_\nu} \tag{4}$$

where the term $T_{bo}e^{-\tau_\nu}$ takes account of the quiet Sun.

The equations (3) and (4) were used for calculations. Because of strong anisotropy the medium was to be divided on thin isotropic sheets. Step of integration varied as an increment of optical depth did not exceed at any step a specified value (0.01 for the presented calculations). At any step the expressions for the calculation of the coefficient of absorption in isotropic medium with averaged parameters of corresponding thin sheet were used, these expressions are described below. As well, at every step the conditions of the QT-inversion had been checked: if emission passed through the QT region of magnetic field and if the wavelength of emission exceeded a critical value. After fulfilment of these conditions the mode of emission had been changed and the increment of optical depth and of brightness temperature were added to the ones of the opposite mode.

To take into account the combined action of several mechanisms of emission (up to three mechanisms) the total coefficients of absorption κ was calculated as a sum of coefficient of absorption of each mechanisms κ_1, κ_2, κ_3:

$$\kappa_\nu = \kappa_{\nu 1} + \kappa_{\nu 2} + \kappa_{\nu 3} \tag{5}$$

For thermal medium the effective temperature of emission is equaled to the kinetic temperature of electrons, but for the non thermal electron distribution (non-maxwellian) the effective temperature is a function of frequency and of mode. For the sources having the non thermal electrons in addition to the thermal electrons the effective temperatures T_{eff1}, T_{eff2} T_{eff3} for 3 several mechanisms of emission were different, and the following weighted average value of the effective temperature were substituted to the equation (4):

$$T_{eff} = k\frac{\nu^2}{c^2}\frac{\eta_\nu}{\kappa_\nu} = k\frac{\nu^2}{c^2}\frac{\eta_{\nu 1} + \eta_{\nu 2} + \eta_{\nu 3}}{\kappa_{\nu 1} + \kappa_{\nu 2} + \kappa_{\nu 3}} =$$

$$= \frac{T_{eff1}\kappa_{\nu 1} + T_{eff2}\kappa_{\nu 2} + T_{eff3}\kappa_{\nu 3}}{\kappa_{\nu 1} + \kappa_{\nu 2} + \kappa_{\nu 3}} \tag{6}$$

where η_ν is total emissivity, and $\eta_{\nu 1}$, $\eta_{\nu 2}$, $\eta_{\nu 3}$ are emissivities of each mechanisms of emission. The integration of the transfer equation were curried either up to the photosphere level or up to the optical depth value $\tau = 20$.

B. Plasma waves scattering

Emission transfer in a plane layer atmosphere with absorption coefficient μ, scattering coefficient σ and indicatrix of scattering $x(\gamma)$ is described by the following equation (Sobolev, 1956):

$$Cos\theta\frac{dI(\tau,\theta)}{d\tau} = I(\tau,\theta)\frac{\sigma}{\mu+\sigma}\int I(\tau,\theta)x(\gamma)\frac{d\Omega}{4\pi} - \frac{\mu}{\mu+\sigma}I_0(\tau) \qquad (7)$$

Here $I(\tau,\theta)$ - intensity of radiation at optical depth τ and at angle θ between direction of a radiation path and direction to the observer, $I_0(\tau) = \epsilon/\mu$, ϵ - an emission coefficient, $d\Omega$ - an element of a solid angle, $d\tau = -(\mu+\sigma)dr$, the coordinate r is directed to the observer, and $\tau = \int\limits_r^\infty(\mu+\sigma)dr$ is directed into solar atmosphere. It is obvious, that $\tau = \tau_\mu + \tau_\sigma$, where τ_μ is the pure absorption optical depth, and τ_σ - the pure scattering optical depth.

In case of a homogeneous layer $\epsilon, \mu, \sigma = const$ by a thickness l and under conditions on the outside boundary $I(0,\pi) = I_2$, and on the interior boundary $I(\tau, 0) = I_1$ it is possible to receive an exact solution of the equation (7) by a method Schwarzschild-Schuster (Sobolev, 1956). At a spherical indicatrix of scattering $x(\gamma)$ this solution has an aspect (Korzhavin, 1994):

$$\begin{aligned} I = I_1 4\beta e^{-\alpha}/q + I_2(1-\beta^2)(1-e^{-2\alpha})/q + \\ +2I_0[\beta(1-e^{-\alpha})](1+\beta-(1-\beta)e^{-\alpha})/q \qquad (8) \end{aligned}$$

Here $\alpha = \sqrt{\tau_\mu(\tau_\mu+\tau_\sigma)} = L\sqrt{\mu(\mu+\sigma)}$, $\beta = \sqrt{\tau_\mu/(\tau_\mu+\tau_\sigma)} = \sqrt{\mu/(\mu+\sigma)}$, $Q = (1+\beta)^2 - (1-\beta)^2e^{-2\alpha}$. Factor at I_1 describes a diffuse passage of the layer, and at I_2 - diffuse reflection from the layer. Factor at I_0 describes an proper radiation of the layer. The square brackets in the formula (8) choose a term, defining basic modification of factor at I_0.

Note that at $\sigma \ll \mu$ the formula (8) passes in an usual solution:

$$I = I_1 e^{-\tau_\mu} + I_0(1-e^{-\tau_\mu}) \qquad (9)$$

Going out from the layer in direction to the observer the radiation I essentially varies at $\tau_\sigma \gg \tau_\mu$, thus in the formula (8) $\alpha \simeq \sqrt{\tau_\mu\tau_\sigma}$, $\beta \simeq \sqrt{\tau_\mu/\tau_\sigma} \ll 1$. Let us consider, that the radiation falling on the layer from a direction of the observer is insignificant, i.e. $I_2 = 0$, and optical thickness of the layer on pure scattering $\tau_\sigma > 1$. In this case, when $\alpha \ll 1$, (8) is reduced to:

$$I = I_1/(1+\tau_\sigma/2) + I_0\tau_\mu \tag{10}$$

As it is visible from (10) radiation, taking place through the layer, I_1 is loosen proportionally its optical thickness on pure scattering τ_σ, on an own radiation of the layer the scattering does not influence in any way. In this case spreading (increasing of sizes) of radiation sources I_1 (Kaplan and Tsytovich, 1972) also should take place. And this effect could be rather more strong then an influence of the interplanetary medium (Bastian, 1994).

In case, when $\alpha \gg 1$, (8) is reduced to:

$$I = 2I_0\beta \tag{11}$$

At $\beta = \sqrt{\tau_\mu/\tau_\sigma} \ll 1$, the own radiation of a layer decreases essentially because of processes of scattering. Obviously, at $\alpha = 1 = \sqrt{\tau_\mu\tau_\sigma}$, the spectral characteristics of the own radiation of a layer should be significantly changed.

The solutions of the transfer equation (7) in simple case of a homogeneous layer ((9), (10), (11)) are well known and are described, for example, in (Zheleznyakov, 1997). (Kaplan and Tsytovich, 1972) have pointed that in turbulence plasma in a radio range the powerful scattering of radio waves on waves of a plasma turbulence should happen. They have derived expressions for scattering coefficients of radio waves on various types of waves of a plasma turbulence. Our observational data do not allow to identify a type of waves of a plasma turbulence, but they show a strong frequency dependence of scattering coefficient. For an example we show equation for a scattering coefficient σ_l of radio waves on a Langmuir turbulence according to (Kaplan and Tsytovich, 1972) :

$$\sigma_l = 1.2\cdot 10^{-28}\lambda^4\ N_e^{5/2}\ T_e^{-1/2}\frac{W_l}{W_{th}} \tag{12}$$

in a range of wavelengths 2 cm $< \lambda <$ 10 cm,
and

$$\sigma_l = 6.5\cdot 10^{-21}\ N_e^{1/2}\ T_e^{3/2}\frac{W_l}{W_{th}} \tag{13}$$

for wavelengths $\lambda > 20$ cm.

According to our observations it is possible to suppose, that for halo the absorption and emission coefficients are defined by a sum of free-free (ff) and nonthermal gyrosyncrotron (gs) mechanisms of a radio emission: $\mu = \mu_{ff} + \mu_{gs}$; $\epsilon = \epsilon_{ff} + \epsilon_{gs}$. At wavelengths $2-3$ cm $\epsilon_{ff} > \epsilon_{gs}$, and on longer waves $\epsilon_{ff} < \epsilon_{gs}$. Since equilibrium intensities for these mechanisms $I_0^{ff} = \epsilon_{ff}/\mu_{ff} \ll I_0^{gs} = \epsilon_{gs}/\mu_{gs}$, then $\mu_{ff} \gg \mu_{gs}$ in full range of observations.

The turning point (maxima) of a gyrosyncrotron spectrum of the halo flux happens at $\lambda = 5$ cm, i.e. at this wave $\alpha = \sqrt{\tau_\mu \tau_\sigma} = 1$. At 2 – 3 cm using observed brightness temperature of halo one can estimate the optical thickness, as $\tau_\mu = T_b/T_e = 0.003$. As τ_{ff} is proportional λ^2, then at $\lambda = 5cm$ $\tau_\mu = \tau_{ff} = 0.1$, and $\tau_\sigma = 10$. Taking into account a size of the radiation source it is possible to estimate σ. Using equation (12) we calculate the ratio of a density of an energy of plasma waves W_l to a density of an energy of thermal plasma $W_{th} = kN_eT_e$ corresponding to the estimated σ. This ratio is $W_l/W_{th} = 10^{-4} - 10^{-5}$, that is a small value (1-10%) from the density of energy nonthermal electrons W_{gs}, necessary for explanation of the growing halo spectrum in a range 1 – 5 cm.

At wavelengths $\lambda > 5$ cm $\alpha = \sqrt{\tau_\mu \tau_\sigma} > 1$. The scattering inside the halo substance at these wavelengths is so great, that according to (11) it causes to strong depressions of own halo radiation and to large halo opacity for a radiation of underlying sources. In a narrow range of wavelengths from 3 up to 5 cm, where τ_σ of halo varies from 1 up to 10 proportionally λ^4 agrees (12), the halo substance is semitransparent for a passing radiation (10). The visibility of underlying sources is sharply worsened in this range relative to shorter wavelengths, and their visible sizes can be much greater then their true sizes.

Acknowledgements

We thank Dr. V.Borovik, Dr. V.Garaimov and Dr. S.White for their help in preparation of this paper. This work has been supported by RFBR grant 03-02-17528.

References

Abramov-Maksimov V.E., V.N. Borovik, V.M. Bogod, G.B. Gelfreikh, V.I. Garaimov, and A.N. Korzhavin, Magnetosphere of the Active Region Based on Multifrequency Solar Observations with New Panoramic Spectra Analyser on RATAN-600. XXIV General Assembly of the URSI, Kyoto, japan, August 25-September 2, 1993. Abstract booklet, Kyoto, 1993, 468.

Akhmedov Sh.B., V.M. Bogod, V.N. Borovik, R. Vilson, G.B. Gelfreikh, V.N. Dikij, A.N. Korzhavin, K.R. Lang, and Z.E. Petrov: 1987, *Astrofis. Issled. (Izv.SAO)*, **25**, 105

Sh.B. Akhmedov, G.B. Gelfreikh, V.M. Bogod, and A.N. Korzhavin, 1982, *Solar Phys.*, **79**, 41

Alissandrakis C. E. and P. Preka-Papadema, 1984, *Astron. Asrtophys.*, **139**, 507

Bandiera R., 1982, *Astron. Astrophys.*, **112**, 52
Bastian T.S., 1995, *ApJ*, **439**, 494
Borovik V.N. and N.G. Peterova, 1987, *Solnechnye dannye (in russian)*, **1**, 66
Cohen M.H., 1960, *Ap.J.*, **131**, 664
Dulk G.A., 1985, *Ann. Rev. Astron. Asrtophys.*, **23**, 169
Dulk G.A. and K.A.Marsh, 1982, *Ap.J.*, **259**, 350
Zheleznyakov V.V. and E.Ya. Zlotnik, 1963, *Astronomicheskii zhurnal (in russian)*, **40**, 633
Zheleznyakov V.V., 1964, *Radioizluchenie Solnza i planet (in russian)*, Moskow, Nauka
Zheleznyakov V.V., 1997, *Izluchenie v astrofizicheskoi plazme (in russian)*, Moskow, Yanus-K
Kaltman T.I., A.N. Korzhavin, N.G. Peterova, B.I. Lubyshev, V.P. Maksimov, C. Alissandrakis, and Q. Fu, 1998, Astronomical Society of the Pacific Conference Series, Second Advances in Solar Active regions, ed. C.Alissandrakis and B.Schmieder, **155**, 140
Kaplan S.A. and V.N. Tsytovich, 1972, Plazmennaya astrophyzika, Moskow, Nauka
Korzhavin A.N. and N.G. Peterova, 1992, thesys of Conference on Radio astronomy investigations of Solar system, ., 14
Korzhavin, A.N. *Nonthermal sources of the microwave emission of active regions in the Sun.* PhD thesis, St-Petersburg, Russia, 1994.
Kruger A., 1976, *Phys.Solariters.*, **N1**, 7
Kucera T.A., G.A. Dulk, D.E. Gary, and T.S. Bastian, 1994, *ApJ*, **433**, 875
Kundu M.R., Solar radio astronomy, Michigan: Ann Arbor, 1964, **1 - 2**
Maksimov V.P. and I.A. Bakunina, *Astronomicheskii zhurnal (in russian)*, 1991, **68**, 394
Peterova N.G. and Sh.B. Akhmedov, 1973, *Astronomicheskii zhurnal (in russian)*, **50**, 1220
Peterova N.G., 1994, *Bull.Spec. Astrophys. Obs.*, **39**, 138
Peterova N.G., 1997, thesis of XXVII radio astronomy conference on Problems of modern radio astronomy (in russian), S.-Petersburg, IPA, **2**, 34
Piddington J.H. and H.C. Minnett. 1951, *Astr. J. Sci.Res.*, **A4**, 131
Sobolev V.V. *Perenos luchistoi energii v atmosferakh zvezd i planet (Radiation energy transfer in atmospheres of stars and planets, in russian).* oskow, Nauka, 1956.
Sych R.A., A.M. Uralov, and A.N. Korzhavin, 1993, *Solar Phys.*, **144**, 59
Tanaka X. and T. Kakinuma, 1959, Paris Symposium on Radio Astronomy, Stanford Univ. Press, 215
Tanaka H. and T. Kakinuma, 1960,*Proc.Res. Inst. Atm. Nagoya Univ.*, **7**, 79
Tsytovich V.N. and S.A. Kaplan, 1968, Astrofizika (in russian),**4**, 3, 332
Solnechnye Dannye, 1988, **10**